Cell Reports
Physical Science

CellPress
OPEN ACCESS

Article

Full Daytime Sub-ambient Radiative Cooling in Commercial-like Paints with High Figure of Merit

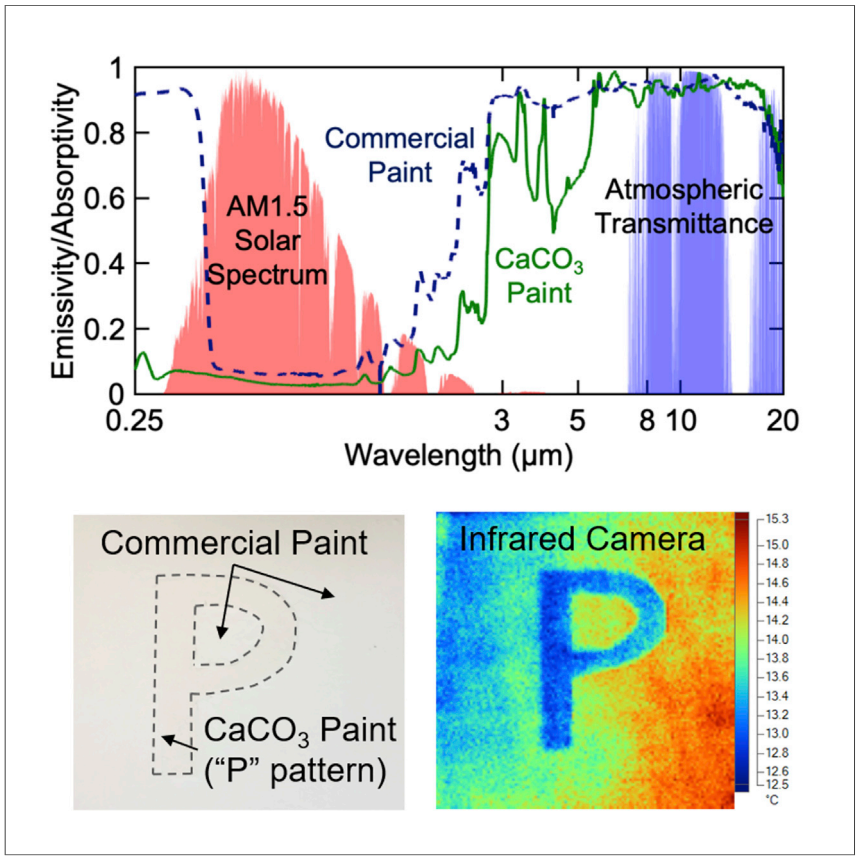

Radiative cooling is a passive cooling technology that can lower cooling costs and mitigate global warming. Recent studies usually use multilayers with a reflective metallic layer. This work by Li et al. demonstrates full daytime sub-ambient cooling in commercial-like single-layer particle-matrix paint with low cost.

Xiangyu Li, Joseph Peoples, Zhifeng Huang, Zixuan Zhao, Jun Qiu, Xiulin Ruan

ruan@purdue.edu

HIGHLIGHTS

Paint using $CaCO_3$ fillers with high concentration and broad particle size

The paint shows a high solar reflectance of 95.5% and sky window emissivity of 0.94

Field test shows >37 W/m^2 cooling power and >1.7°C below ambient at noon

Commercial-like paint offers a high standard figure of merit of 0.49

Li et al., Cell Reports Physical Science 1, 100221
October 21, 2020
https://doi.org/10.1016/j.xcrp.2020.100221

Cell Reports
Physical Science

CellPress
OPEN ACCESS

Article

Full Daytime Sub-ambient Radiative Cooling in Commercial-like Paints with High Figure of Merit

Xiangyu Li,[1,2] Joseph Peoples,[1,2] Zhifeng Huang,[1,3] Zixuan Zhao,[1] Jun Qiu,[1,4,5] and Xiulin Ruan[1,2,6,*]

SUMMARY

Radiative cooling is a passive cooling technology that acts by reflecting sunlight and emitting radiation in the sky window. Although highly desirable, full daytime sub-ambient radiative cooling in commercial-like single-layer particle-matrix paints has not been achieved. Here, we demonstrate full daytime sub-ambient radiative cooling in $CaCO_3$-acrylic paint by using large band gap $CaCO_3$ fillers, a high particle concentration of 60%, and a broad size distribution. Our paint shows a high solar reflectance of 95.5% and a high normal emissivity of 0.94 in the sky window. Field tests show cooling power exceeding 37 W/m^2 and a surface temperature of >1.7°C below ambient at noon. A figure of merit RC is proposed to compare the cooling performance independent of weather conditions. The standard RC of our paint is 0.49, among the best radiative cooling performances, while offering the benefits of convenient paint form, low cost, and compatibility with commercial paint fabrication processes.

INTRODUCTION

Cooling represents a significant sector of energy consumption in both residential and commercial applications.[1] Passive radiative cooling can cool surfaces without any energy consumption by directly emitting heat through a transparent spectral window of the atmosphere, from 8 to 13 μm (the "sky window"), to the deep sky, which functions as an infinite heat sink, with a temperature of 3 K. By "sky window," we particularly mean 8 to 13 μm, which is also the widely used convention. Other sky windows could be specified such as the second sky window, and so forth. If the thermal emission of the surface through the sky window exceeds its absorption of the sunlight, then the surface can be cooled below the ambient temperature under direct sunlight. Compared to conventional air conditioners that consume electricity and only move heat from the inside of the space to the outdoors, passive radiative cooling not only saves power but it also combats global warming since the heat is directly lost to the deep space.

The use of passive radiative cooling dates back centuries,[2] and scientific studies on radiative cooling started as early as the 1960s.[3–9] Paints with sub-ambient daytime radiative cooling capability have long been pursued,[10–15] and TiO_2 particles, the common pigments in commercial paints, were used in most of these studies. The particle size was usually selected to be on the order of hundreds of nanometers to several microns, since light can be strongly scattered and reflected by particles with a size comparable to the wavelength.[16–18] A thin layer of TiO_2 white paint coated on aluminum demonstrated daytime below-ambient cooling during a winter day, and the high solar reflectance was attributed to the aluminum substrate.[10] Recently, full daytime sub-ambient cooling has been demonstrated in photonic

[1]School of Mechanical Engineering, Purdue University, West Lafayette, IN 47907, USA

[2]Birck Nanotechnology Center, Purdue University, West Lafayette, IN 47907, USA

[3]School of Power and Mechanical Engineering, Wuhan University, Wuhan 430072, China

[4]School of Energy Science and Engineering, Harbin Institute of Technology, Harbin 150001, China

[5]State Key Laboratory for Digital Manufacturing Equipment and Technology, Huazhong University of Science and Technology, Wuhan 430074, China

[6]Lead Contact

*Correspondence: ruan@purdue.edu

https://doi.org/10.1016/j.xcrp.2020.100221

structures and multilayers,[19,20] which renewed interest in the development of various radiative cooling materials. A subset of the authors theoretically predicted full daytime sub-ambient cooling using a dual-layer structure with TiO_2-acrylic paint layer on top of a carbon black layer,[13] or using a broad particle size distribution instead of a single size to enable efficient broadband scattering of sunlight.[21] However, these theoretical proposals have not been experimentally confirmed. In fact, the performance of TiO_2-acrylic paints is limited by solar absorption in the ultraviolet (UV) band due to the moderate 3.2 eV electron band gap of TiO_2 and the near-infrared (NIR) 0.7- to 3-μm band due to acrylic absorption.[21] Theoretical studies have indicated that the solar reflectance of TiO_2-acrylic paint is unlikely to exceed 92%.[13,21] Other materials with higher band gaps, such as SiO_2,[15] ZnS,[22] and $BaSO_4$,[23] have been studied to reduce the UV absorption, while a drawback is their lower refractive indices compared to that of TiO_2, which hurts scattering. Among these, a single-layer SiO_2 particle bed was developed and partial daytime sub-ambient cooling was demonstrated, except for the noon hours.[15] A recent review paper on existing commercial heat-reflective paints notes that their solar reflectance is moderately high, ~80% to 90%, and none of the paints has achieved full daytime sub-ambient cooling.[12] However, porous structures have also been explored to enhance solar reflectance,[24–26] and a recent study based on porous polymers accomplished daytime cooling and they are paint-like.[27] Other non-paint daytime radiative cooling solutions include a polymer-metal dual layer,[28,29] a silica nanocomposite-metal dual layer,[30] a silica-metal dual layer,[31] and delignified wood.[32] Taking these existing studies into consideration, it is clear that it is still a pertinent and challenging task to create single-layer commercial-like nanoparticle-matrix paint for daytime radiative cooling that can gain wide commercial application.

In this work, we experimentally demonstrate high solar reflectance, high normal emissivity in the sky window, and full daytime sub-ambient radiative cooling in single-layer particle-matrix paints with strong performance. The results are also included in a provisional patent filed on October 3, 2018 and a non-provisional international patent application (PCT/US2019/054566) filed on October 3, 2019 and published on April 9, 2020.[33] Our work is enabled by the use of several different approaches from commercial paints: the large band gap $CaCO_3$ fillers, a high particle concentration of 60%, and a broad size distribution. Our paint shows a high solar reflectance of 95.5% and a high normal emissivity of 0.94 in the sky window. Field tests demonstrate cooling power exceeding 37 W/m^2 and a surface temperature >1.7°C below ambient at noon. A figure of merit RC is proposed to compare the cooling performance independent of weather conditions. The standard RC of our cooling paint is 0.49, among the best radiative cooling performance reported, while offering unprecedented benefits of the convenient paint form, low cost, and compatibility with commercial paint fabrication processes.

RESULTS AND DISCUSSION

Fabrication and Optical Properties of the Cooling Paint

We design our paint with a systematic approach by considering multiple factors. To minimize the solar absorption in the UV band, we consider and investigate many alternative materials with higher electron band gaps, and achieve strong performance with $CaCO_3$-acrylic paint, in which $CaCO_3$ has an electronic band gap >5 eV. $CaCO_3$ has also been shown as a compatible and stable material used in paints as spacers,[34] but here it is used for a different purpose. To compensate for its low refractive index[35] and enable strong scattering, we adopt a particle volume concentration of 60%, which is considerably higher than those in commercial

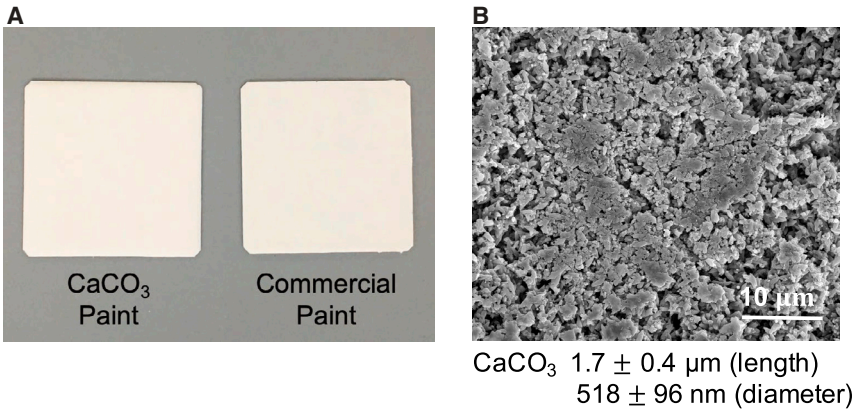

Figure 1. $CaCO_3$-Acrylic Paint

(A) Our freestanding radiative cooling paint sample along with commercial white paint.

(B) An SEM image of the $CaCO_3$-acrylic paint. The particle size distribution is measured from SEM images.

paints. It is known for TiO_2 paints that the optical reflectance increases with the particle concentration up until ~30%, when the optical crowding effect often occurs, and a further increase of particle concentration would lead to an overall decrease in the reflectance.[34] However, as the particle concentration continues to increase and pass the critical particle volume concentration (CPVC), the reflectance will increase again.[34] Hence, we select the 60% concentration, which is well above the CPVC. It also reduces the volume of acrylic and its absorption in the NIR band. Furthermore, a broad particle size distribution instead of a single size is used to efficiently scatter all of the wavelengths in the solar spectrum, and hence enhance the solar reflectance, as predicted in our previous simulations.[21] Finally, the acrylic matrix introduces vibrational resonance peaks in the IR band, thus ensuring a high sky window emissivity.

$CaCO_3$-acrylic paint with 60% volume concentration was made using a commercially compatible process. A mixture of dimethylformamide (DMF), acrylic, and particle fillers was left fully dried. The thickness of the sample was ~400 μm to make the properties substrate-independent. The details are presented in the Experimental Procedures. The freestanding $CaCO_3$ nanoparticle-acrylic paint sample is shown in Figure 1A, along with commercial white paint (Dutch Boy Maxbond UltraWhite Exterior Acrylic Paint, 400 μm thick). The scanning electron microscopy (SEM) image of the sample surface is shown in Figure 1B, in which $CaCO_3$ fillers are rod shaped, ~1.9 μm long, and~500 nm in diameter. Some air voids were introduced when the concentration went beyond the CPVC, and they could have a significant role in increasing the solar reflectance.

The solar reflectance and sky window emissivity were then characterized. To achieve full daytime below-ambient cooling, it is critical to have both high solar reflectance and high sky window emissivity. The solar reflectance is mainly contributed by fillers, and the sky window emission can come from the matrix and/or fillers, as shown in Figure 2A. The high solar reflectance results from a combination of several factors, including filler refractive index, volume concentration, particle size, and size distribution. To compensate for the low refractive index of $CaCO_3$ compared to TiO_2, we set the filler concentration at 60%, which is above the CPVC, to enhance the solar reflectance. Through experimental trials, the 60% filler concentration provided sufficient solar reflectance while maintaining good reliability. For operating temperatures

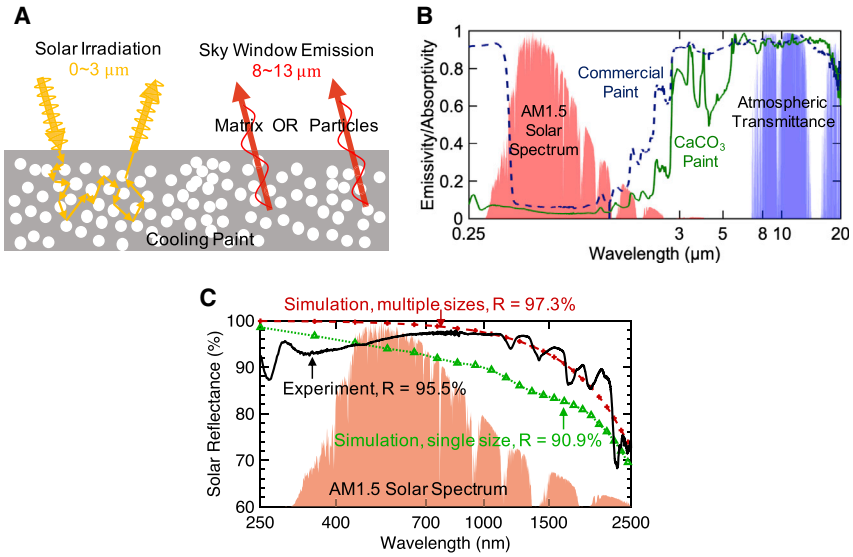

Figure 2. Radiative Cooling Schematic alongside Spectral Characterization and Monte Carlo Simulations

(A) For cooling paints exposed to direct solar irradiation, the fillers reflect sunlight between 0 and 3 μm, and the particles and/or polymer matrix emit in the sky window between 8 and 13 μm.

(B) The normal emissivity of our radiative cooling paint characterized from 0.25 to 20 μm, compared with commercial white paint.

(C) Monte Carlo simulations of the solar reflectance of the $CaCO_3$-acrylic paint at 60% concentration compared with experimental results. Broad size distribution enhances the solar reflectance, and the results are in good agreement with the experimental measurement (black line).

close to 300 K, the dominant spectral range of the sky window is between 8 and 13 μm, and phonon (from the filler) or vibrational (from the polymer matrix) resonance peaks are essential for passive radiative cooling. At those peaks, photons are absorbed while interacting with phonons or vibrons, leading to high absorptivity and emissivity. Since $CaCO_3$ alone has a low emissivity in the 8- to 13-μm spectral range, the high sky window emissivity is mainly contributed by the acrylic matrix. The normal emissivity from 250 nm to 20 μm is shown in Figure 2B. While maintaining a high normal emissivity of 0.94 in the sky window, our $CaCO_3$-acrylic paint reaches 95.5% reflectance in the solar spectrum due to low absorption in the UV and NIR regions, compared to the 87.2% reflectance of the commercial white paint (Dutch Boy Maxbond UltraWhite Exterior Acrylic Paint). Although Dutch Boy paint is not a heat-reflective commercial paint, the solar reflectance of the $CaCO_3$ paint is still substantially higher than those of the commercial heat-reflective paints that show a solar reflectance of ~80%–90%.[12,36] Further comparison between our paint with a wide range of commercial paints is under way.

To help illustrate the physics behind the strong radiative properties, we performed photon Monte Carlo simulations of the nanoparticle composites with a thickness of 400 μm. Due to the ellipsoidal shape of the $CaCO_3$ particles, an effective particle size[37] was used with a diameter μ_d of 517.3 nm with a σ_d of 95.9 nm and a length μ_l of 1744 nm with a σ_l of 408.4 nm. The uncertainty of the measurements was found to be $\pm$15.1 nm. The dielectric function of $CaCO_3$ was obtained from the literature.[35] A modified Lorentz-Mie theory[21] was used to obtain the scattering coefficient η_s, the absorption coefficient η_a, and the asymmetric parameter of the nanoparticles in the matrix. A simple correction was then used to capture the dependent scattering effect due to the high concentration,[38]

$$\eta_{sd} = \eta_s\left(1 + 1.5f - 0.75f^2\right) \quad \text{(Equation 1)}$$

$$\eta_{ad} = \eta_a\left(1 + 1.5f - 0.75f^2\right) \quad \text{(Equation 2)}$$

where f is the particle volume fraction and η_{sd} and η_{ad} are the scattering and absorption coefficients, respectively, after considering dependent scattering. These modified coefficients were then applied to a homogeneous effective medium, where we used the Monte Carlo method to solve the radiative transfer equation by releasing 500,000 photons into the effective medium to predict reflectivity, absorptivity, and emissivity. We covered 226 wavelengths from 250 nm to 2.5 μm. The results are shown in Figure 2C. We observed that using the single average particle size results in a solar reflectance of 90.9%, which is considerably lower than the experimental value. Including the size distribution increases the solar reflectance to 97.3% and agrees with the experimental value much better. Although one single particle size is able to strongly scatter one narrow spectral band, a broad distribution of particle sizes can effectively scatter a larger spectral range, leading to a higher overall solar reflectance. The results support our previous theoretical proposal that multiple particle sizes can effectively scatter the broadband wavelength.[21] The uncertainty from the Monte Carlo simulations is ±0.3%. In addition, the effect of paint thickness is discussed in Note S1 and Figure S1. Thinner films with thicknesses of 98, 131, and 177 μm still provide high solar reflectances of 88.9%, 93.4%, and 95.1%, respectively.

Field Test of the Cooling Performance

A field test of surface temperatures demonstrated full daytime cooling in West Lafayette, Indiana on March 21–23, 2018, as seen in Figure 3A. The sample stayed 10°C below the ambient temperature at night, and at least 1.7°C below the ambient temperature at a peak solar irradiation ~963 W/m^2. The relative humidity at 12 p.m. was ~40% with total precipitable water of 1,613.5 atm-cm. In another demonstration, a "P" pattern was painted with the $CaCO_3$-acrylic paint and the rest was painted with commercial white paint of the same thickness. It was then placed under direct sunlight. As shown in Figure 3B, the pattern was nearly invisible to a regular camera since both paints share high reflectances in the visible spectrum (0.4–0.7 μm). However, it became much more distinctive to an IR camera, clearly showing that the $CaCO_3$-acrylic paint was able to maintain a lower temperature under direct sunlight compared to the commercial white paint. The cooling power measurement using a feedback heater in Figure 3C showed an average cooling power of 56 W/m^2 during nights and 37 W/m^2 at ~12 p.m. (between 10 a.m. and 2 p.m.) in Reno, Nevada on August 1–2, 2018, when the relative humidity was 10% at 12 p.m. with total precipitable water of 1,755.7 atm-cm. A detailed analysis of the cooling power and comparison to experimental data are provided in Note S2 and Figures S2 and S3.

Figure of Merit

In the literature,[20,27,28,30,31] and thus far in this work, cooling powers were reported for different locations and weather conditions. In fact, the weather conditions can critically affect the cooling power. For instance, humid weather can significantly reduce the cooling power compared to dry climates.[39] Although considering these various factors is very important when a radiative cooling material moves down to the application stage, it makes it hard to fairly assess different radiative cooling systems under similar conditions. Hence, it is beneficial to introduce a metric that can provide an initial assessment of the radiative cooling of a material. Here, we define a simple figure of merit, RC, to help unify the radiative cooling performance by using the same ideal weather condition:

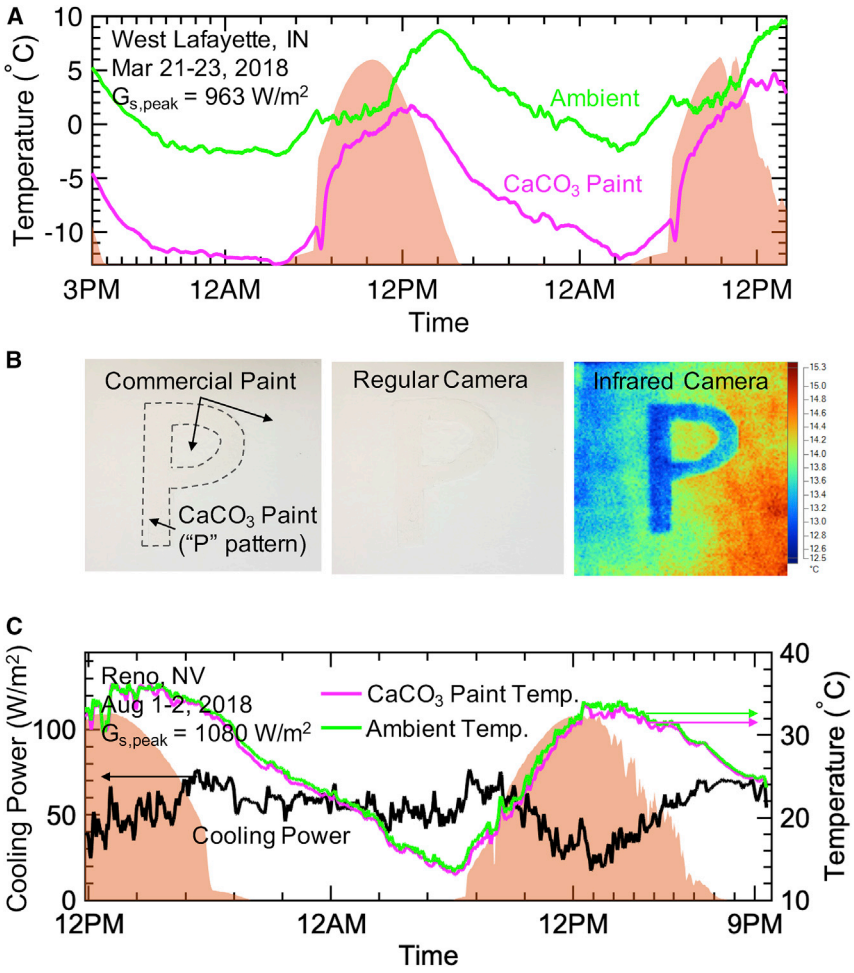

Figure 3. Field Tests of the Cooling Paint

(A) Field temperature measurement for the $CaCO_3$-acrylic paint over a period of >1 day.

(B) A "P" pattern painted with the $CaCO_3$-acrylic paint and the rest with the commercial white paint was placed under direct sunlight. The pattern was nearly invisible to a regular camera but became much more distinctive to an infrared (IR) camera due to the lower temperature of the $CaCO_3$-acrylic paint.

(C) Cooling power directly measured for the $CaCO_3$-acrylic paint using a feedback heater.

The orange regions stand for the solar irradiation intensity in (A) and (C).

$$RC = \varepsilon_{Sky} - r(1 - R_{Solar}) \quad \text{(Equation 3)}$$

where ε_{Sky} is the emissivity in the sky window, R_{Solar} is the total reflectance in the solar spectrum, and r is the ratio of the solar irradiation power over the blackbody surface emissive power transmitted through the sky window. Multiplying RC by the blackbody surface emissive power transmitted through the sky window would yield the net cooling power when the surface temperature is synced to the ambient. RC can be calculated to fairly evaluate different radiative cooling systems at the same solar irradiation and weather conditions. We recommend defining a "standard RC" by using a standard surface temperature of 300 K to calculate ε_{Sky} and using a standard r value of 10 (assuming a typical peak solar irradiation of 1,000 W/m^2 and typical blackbody surface emissive power transmitted through the sky window of 100 W/m^2). An ideal surface with 100% solar reflectance and an emissivity of 1 in the sky window has an RC of 1. Here, we can also see that due to the higher solar

intensity compared to the sky window emissive power, achieving higher solar reflectance is the key to enhancing the overall cooling power and RC. The standard figures of merit for the commercial white paint used in this study and our $CaCO_3$-acrylic paint are −0.33 and 0.49, compared to other state-of-the-art non-paint approaches as 0.32,[20] 0.53,[30] 0.35,[31] and 0.57.[27] The RC of our $CaCO_3$-acrylic paint is comparable to or better than these reported radiative cooling systems. If the figure of merit is positive, the surface should be able to provide a sub-ambient cooling effect. It is recommended that our standard figure of merit is used for an initial assessment of the potential of the material for radiative cooling, especially when the ideal dry and summer days are not accessible for researchers to perform field tests. We should note that our standard figure of merit is defined at a surface temperature of 300 K and a set of representative conditions. It will not differentiate between hemispherical versus near-normal emittance or selective versus broadband emitters. For example, the solar adsorption will have a more significant role, and hence a higher r value under more humid conditions, when the blackbody surface emissive power transmitted through the sky window can be significantly reduced below 100 W/m^2. However, in a very dry and hot climate, the r value can be quite lower than 10 due to the blackbody surface emissive power transmitted through the sky window significantly exceeding 100 W/m^2. Furthermore, a broadband emitter will perform better than a selective surface under high operating temperatures even with the same figure of merit. Therefore, once the material is moved down to the application stage, field tests should be performed, and modified figure of merits can be defined based on the specific application, location, weather, cost, and so forth. We note that a solar reflectance index (SRI) is widely used for paints.[40] Our RC is not intended to replace the SRI, but instead to offer a complementary figure of merit specifically for assessing the radiative cooling performance of different systems.

Reliability Tests, Viscosity Characterization, and Cost Analysis

Abrasion tests were performed with the Taber Abraser Research Model according to ASTM D4060.[41] A pair of abrasive wheels (CS-10) were placed on the surface with a 250-g load per wheel. The mass loss was measured every 250 cycles and the refacing was done every 500 cycles as required. The wear index (I) is defined as the weight loss in the unit of milligrams per 1,000 cycles as

$$I = \Delta m \times 1000/C \qquad \text{(Equation 4)}$$

where Δm is the weight loss and C is the cycle number. Using a linear fit to the mass loss, Figure 4A shows that the wear indexes of the commercial exterior paint and $CaCO_3$ paint are 104 and 84, respectively. Overall, our cooling paint showed similar abrasion resistance compared to the commercial exterior paints. In a weathering test, the $CaCO_3$ paint was exposed to outdoor weathering, including rain and snow, for ~3 weeks. Figure 4B shows that the solar reflectance remained within the uncertainty level during the testing period. The sky window normal emissivity remained at 0.94 at the beginning and the end of the test. Video S1 of a running water test is provided to illustrate that our paint is water resistant. The acrylic matrix strongly bonds the $CaCO_3$ fillers together, which helps to reduce the damage from exterior abrasion and outdoor weathering. Nevertheless, a long-term reliability test is under way, including UV exposure, dust, surface adhesion, and water/detergent resistance. Due to the air voids introduced in the paint, it is also important to conduct reliability tests with regard to possible penetration by acidic water in future studies.[42] The viscosity of the $CaCO_3$ paint was measured and compared with water- and oil-based commercial paints in Figure 4C. The viscosity of the commercial paints was retrieved from Whittingstall's work.[43] Our $CaCO_3$ paint showed lower viscosity, indicating that it can be brushed and dried similarly to commercial paints, as

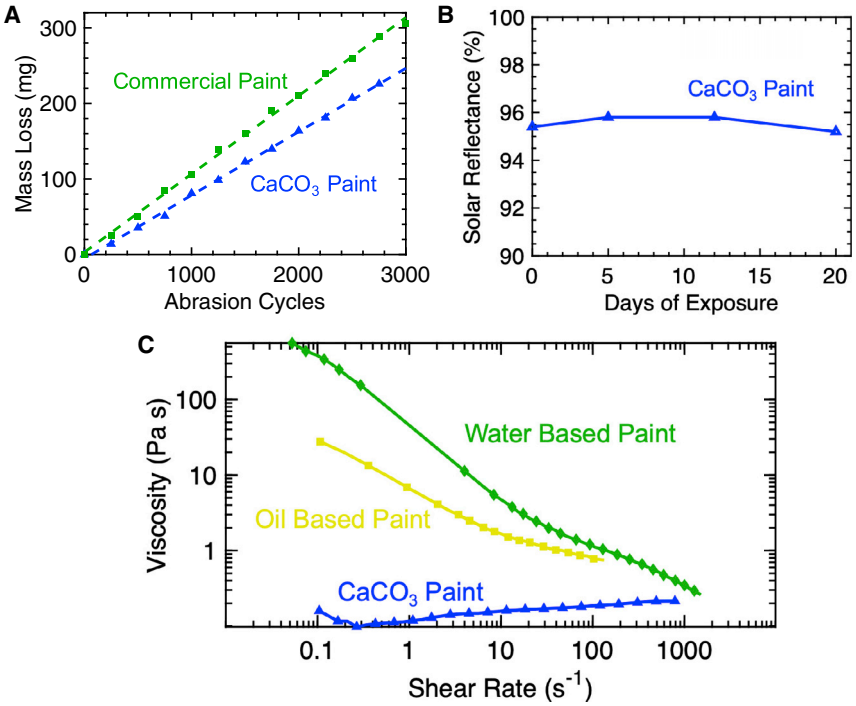

Figure 4. Abrasion and Viscosity Characterizations of the Cooling Paint

(A) The mass loss as a function of the cycle number in abrasion tests. The slope retrieved was used to calculate the wear index.

(B) The solar reflectance remained the same during the 3-week outdoor weathering test.

(C) The viscosity of the cooling paint was compared to that of commercial paints.[43]

demonstrated by Video S1. The viscosity can be further adjusted by changing the type and amount of solvent used.

Due to the wide availability of $CaCO_3$ in natural minerals, the cost of our radiative cooling paints is anticipated to be comparable to or even lower than that of commercial white paints. The cost of the particle fillers for covering a 100-m^2 area is <$1.50 for $CaCO_3$ paint, making them among the most cost-effective radiative cooling solutions with full daytime below-ambient cooling capability. Since our $CaCO_3$ paint is compatible with commercial paint, the fabrication, labor, and safety cost of the paint will be similar to current commercial paints as well. The Heat Island group at the Lawrence Berkeley National Laboratory has performed comprehensive tests with 85% solar reflectance roofing materials and concluded their energy savings to be 40–75 Wh/m^2/day on different buildings during a 1-month period in the summer.[44] Our cooling paints showed a better performance, with >95% solar reflectance. With the total solar irradiation ~5,000 Wh/m^2/day, our paint can produce an energy savings of 70–105 Wh/m^2/day, assuming the alternating current (AC) stock average efficiency to be 15. If the electricity cost is set at $0.1/kWh, then the savings on the cooling costs will be $0.7/day for a moderate 100-m^2 apartment.

In summary, we have demonstrated that $CaCO_3$-acrylic paint, with a high particle concentration and a broad size distribution, is able to achieve full daytime below-ambient cooling with a high standard figure of merit of 0.49. The intrinsic large band gap, appropriate particle size, broad particle size distribution, and high particle concentration are essential to strongly reflect the sunlight. The vibrational resonance peaks of the acrylic matrix provide strong emission in the sky window. Our

radiative cooling paint showed a cooling performance that was among the best of the reported state-of-the-art approaches, while offering unprecedented combined benefits, including convenient paint form, low cost, and compatibility with commercial paint fabrication processes. Future studies can aim at achieving greater performance with thinner films by exploring materials and structures. During the review process of our paper, we were made aware that results similar to part of our work (i.e., high solar reflectance in paints embedded with high concentration-wide band gap particles) were also reported in another article[45] published while our paper was under review.

EXPERIMENTAL PROCEDURES

Resource Availability

Lead Contact

Dr. Xiulin Ruan: ruan@purdue.edu.

Materials Availability

This study did not generate new unique reagents.

Data and Code Availability

All of the data associated with the study are included in the article and the Supplemental Information. Original data have been deposited to Mendeley Data: https://doi.org/10.17632/gvxxr8j62w.1. Additional information is available from the Lead Contact upon reasonable request.

Sample Fabrication

The $CaCO_3$ particles were mixed with DMF first, followed by a 10-min sonication to reduce particle agglomerations. We used Elvacite 2028 from Lucite International as the acrylic matrix because of its low viscosity. The acrylic was then slowly added to the mixture to dissolve. The mixture was later degassed in a vacuum chamber to remove air bubbles introduced during mixing and ultrasonication. The mixture was then poured in a mold and dried overnight until all of the solvent was gone. The dried paint was released from the mold as a freestanding layer with a thickness of $\sim$400 μm.

Optical Measurement

The solar reflectance was measured on a PerkinElmer Lambda 950 UV-VIS-NIR spectrometer with an integrating sphere, using a certified Spectralon diffuse reflectance standard. The effective solar reflectance was calculated based on the reference AM 1.5 solar spectra.[46] The uncertainty was $\pm$0.5% based on the results of 5 different samples made in separate batches. Additional calibrations were done with a silicon wafer, and the solar reflectance of the $CaCO_3$-acrylic paint was 94.9%, which is consistent with that from the diffuse reflectance standard. The IR measurements were done on a Nicolet iS50 Fourier transform IR (FTIR) spectrometer with a PIKE Technologies integrating sphere for a near-normal incidence. The true hemispherical emittance can be 2%–3% lower for rough surfaces when estimating the heat loss. The uncertainty of the PIKE Technologies diffuse reflectance standard was $\pm$0.02. The atmospheric transmittance is under the condition of air mass 1.5 and water vapor column 1.0 mm (IR Transmission Spectra, Gemini Observatory).

Field Test Setups

Two field test setups were made to characterize the cooling performance of the paints on the roof of a high-rise building, as shown in Figure 5. Figure 5A is a temperature test setup to demonstrate the below-ambient cooling capability. A cavity

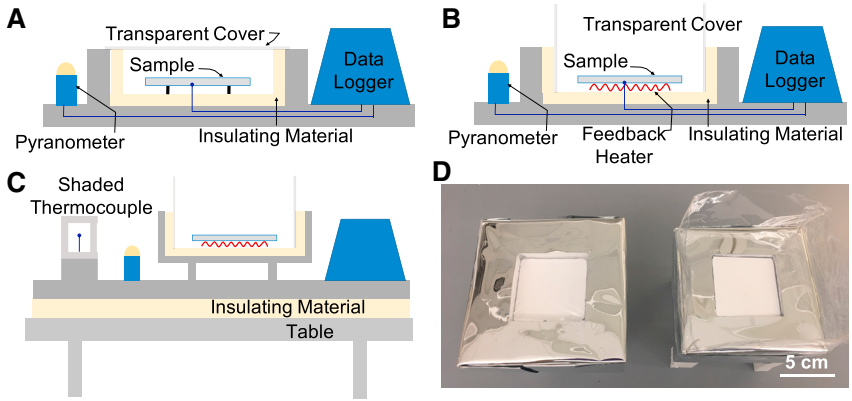

Figure 5. Field Test Setups for Cooling Performance Characterization

(A) A temperature test setup in which the temperatures of the sample and the ambient were recorded. A lower sample temperature than the ambient indicated below-ambient cooling.

(B) A cooling power test setup in which the sample was heated to the same temperature as the ambient using a feedback heater. The power consumption of the heater was equal to the cooling power.

(C) The setups were further placed on a high-rise table to eliminate the heating effect from the ground. A shaded thermocouple was located at a similar height to the cooling samples to avoid overheating from the ground.

(D) Pictures of actual setups. On the left and right are temperature and cooling power test setups, respectively.

was made from a block of white Styrofoam, which provided excellent insulation from heat conduction. The 5-cm^2 sample was suspended above the Styrofoam base. A thin layer of low-density polyethylene (LDPE) film was used as a shield against forced convection. T-type thermocouples were attached to the bottom of the samples to measure temperatures. An additional shaded thermocouple outside the setup was used to monitor the ambient temperature. A pyranometer was placed to measure the solar irradiation, including both direct and diffuse components. According to the manufacturer, the accuracy depends on the angle of the irradiation, with directional errors <20 W/m^2 at an 80 solar zenith angle. Figure 5B shows the cooling power test setup. A feedback heater was attached to the back of the sample to synchronize the sample and ambient temperatures. As the sample was heated to the ambient temperature, the power consumption of the heater was recorded as equal to the cooling power. The uncertainty, $\pm$5 W/m^2, was calculated as the standard deviation of measured nighttime cooling power at a stable surface temperature. The conduction and convection losses were insignificant (see details in Note S2). In addition, the setups were located on a wood board, which was further insulated on a metal table above the ground to avoid the heating effect from the ground (Figure 5C). Both setups were covered by silver Mylar to reflect solar irradiation. The actual pictures of the two onsite cooling setups were shown in Figure 5D. The sidewalls and the bottoms of the Styrofoam setups were enclosed by silver Mylar to prevent additional radiation heat transfer.

Monte Carlo Simulations

The Monte Carlo simulations were performed in a manner similar to our previous work,[21] but a correction for dependent scattering was added. The photon packet is released at the top of the interface between the air and the nanocomposite. The photon starts with a weight of unity and a normal direction to the air-composite interface. As the photon propagates across the air-composite interface and through the medium, it will lose weight scaling with the absorbing coefficient and will change

direction affected by the scattering coefficient and asymmetric parameter. If the photon propagates to the bottom interface and makes it through, then that weight is considered transmitted. If the photon propagates back up to the top surface and goes through the interface, then it is considered reflected.

SUPPLEMENTAL INFORMATION

Supplemental Information can be found online at https://doi.org/10.1016/j.xcrp.2020.100221.

ACKNOWLEDGMENTS

The authors thank Mian Wang, Jacob Faulkner, Professor George Chiu, and Professor Zhi Zhou at Purdue University for their help in sample fabrication. They thank Professor Yan Wang at University of Nevada, Reno for assistance on the field tests. This research was supported by the Cooling Technologies Research Center at Purdue University and the Air Force Office of Scientific Research through the Defense University Research Instrumentation Program (grant no. FA9550-17-1-0368).

AUTHOR CONTRIBUTIONS

Conceptualization, X.R.; Methodology, X.R. and X.L.; Software, J.P., Z.H., and J.Q.; Investigation, X.L., J.P., and Z.Z.; Writing – Original Draft, X.R. and X.L.; Writing – Review & Editing, X.R., X.L., J.P., Z.H., J.Q., and Z.Z.; Funding Acquisition, X.R.; Resources, X.R.; Supervision, X.R.

DECLARATION OF INTERESTS

X.R., X.L., Z.H., and J.P. are the inventors of a provisional patent application filed on October 3, 2018 and a non-provisional international patent application (PCT/US2019/054566) filed on October 3, 2019 and published on April 9, 2020.[33]

Received: July 7, 2020
Revised: August 24, 2020
Accepted: September 14, 2020
Published: October 21, 2020

REFERENCES

1. US Energy Information Administration (2018). Annual Energy Outlook 2018 with projections to 2050. J. Phys. A Math. Theor. *44*, 1–64.
2. Barker, R. (1857). Process of Making Ice in the East Indies. Sci. Am. *13*, 75.
3. Catalanotti, S., Cuomo, V., Piro, G., Ruggi, D., Silvestrini, V., and Troise, G. (1975). The radiative cooling of selective surfaces. Sol. Energy *17*, 83–89.
4. Granqvist, C.G., Hjortsberg, A., Granqvist, G., and Hjortsberg, A. (1981). Radiative cooling to low temperatures: general considerations and application to selectively emitting SiO films. J. Appl. Phys. *51*, 4205.
5. Andretta, A., Bartoli, B., Coluzzi, B., and Cuomo, V. (1981). Selective Surfaces for Natural Cooling Devices. J. Phys. Colloq. *42* (C1), C1-423–C1-430.
6. Lushiku, E.M., Hjortsberg, A., and Granqvist, C.G. (1982). Radiative cooling with selectively infrared-emitting ammonia gas. J. Appl. Physiol. *53*, 5526–5530.
7. Lushiku, E.M., and Granqvist, C.-G. (1984). Radiative cooling with selectively infrared-emitting gases. Appl. Opt. *23*, 1835.
8. Diatezua, D.M., Thiry, P.A., Dereux, A., and Caudano, R. (1996). Silicon oxynitride multilayers as spectrally selective material for passive radiative cooling applications. Sol. Energy Mater. Sol. Cells *40*, 253–259.
9. Gentle, A.R., and Smith, G.B. (2010). Radiative heat pumping from the Earth using surface phonon resonant nanoparticles. Nano Lett. *10*, 373–379.
10. Harrison, A.W. (1978). Radiative cooling of TiO2 white paint. Sol. Energy *20*, 185–188.
11. Orel, B., Gunde, M.K., and Krainer, A. (1993). Radiative cooling efficiency of white pigmented paints. Sol. Energy *50*, 477–482.
12. Pockett, J. (2010). Heat Reflecting Paints and a Review of their Advertising Material. In CHEMECA 2010: Engineering at the Edge, *26-29* September, pp. 1–13.
13. Huang, Z., and Ruan, X. (2017). Nanoparticle embedded double-layer coating for daytime radiative cooling. Int. J. Heat Mass Transf. *104*, 890–896.
14. Bao, H., Yan, C., Wang, B., Fang, X., Zhao, C.Y., and Ruan, X. (2017). Double-layer nanoparticle-based coatings for efficient terrestrial radiative cooling. Sol. Energy Mater. Sol. Cells *168*, 78–84.
15. Atiganyanun, S., Plumley, J., Han, S.J., Hsu, K., Cytrynbaum, J., Peng, T.L., Han, S.M., and Han, S.E. (2018). Effective Radiative Cooling by Paint-Format Microsphere-Based Photonic Random Media. ACS Photonics *5*, 1181–1187.
16. Mie, G. (1908). Beiträge zur Optik trüber Medien, speziell kolloidaler Metallösungen. Ann. Physiol. *330*, 377–445.
17. Lorenz, L. (1890). Lysbevægelsen i og uden for en haf plane lysbölger belyst Kulge, Vidensk. Selk. Skr. *6*, 1–62.

18. Song, J., Qin, J., Qu, J., Song, Z., Zhang, W., Xue, X., Shi, Y., Zhang, T., Ji, W., Zhang, R., et al. (2014). The effects of particle size distribution on the optical properties of titanium dioxide rutile pigments and their applications in cool non-white coatings. Sol. Energy Mater. Sol. Cells *130*, 42–50.

19. Rephaeli, E., Raman, A., and Fan, S. (2013). Ultrabroadband photonic structures to achieve high-performance daytime radiative cooling. Nano Lett. *13*, 1457–1461.

20. Raman, A.P., Anoma, M.A., Zhu, L., Rephaeli, E., and Fan, S. (2014). Passive radiative cooling below ambient air temperature under direct sunlight. Nature *515*, 540–544.

21. Peoples, J., Li, X., Lv, Y., Qiu, J., Huang, Z., and Ruan, X. (2019). A strategy of hierarchical particle sizes in nanoparticle composite for enhancing solar reflection. Int. J. Heat Mass Transf. *131*, 487–494.

22. Nilsson, T.M.J., and Niklasson, G.A. (1995). Radiative cooling during the day: simulations and experiments on pigmented polyethylene cover foils. Sol. Energy Mater. Sol. Cells *37*, 93–118.

23. Grum, F., and Luckey, G.W. (1968). Optical sphere paint and a working standard of reflectance. Appl. Opt. *7*, 2289–2294.

24. Syurik, J., Jacucci, G., Onelli, O.D., Hölscher, H., and Vignolini, S. (2018). Biol.-inspired Highly Scattering Networks via Polymer Phase Separation. Adv. Funct. Mater. *28*, 1706901.

25. Zou, W., Pattelli, L., Guo, J., Yang, S., Yang, M., Zhao, N., Xu, J., and Wiersma, D.S. (2019). Biomimetic Polymer Film with Brilliant Brightness Using a One-Step Water Vapor–Induced Phase Separation Method. Adv. Funct. Mater. *29*, 1808885.

26. Leroy, A., Bhatia, B., Kelsall, C.C., Castillejo-Cuberos, A., Di Capua, H.,M., Zhao, L., Zhang, L., Guzman, A.M., and Wang, E.N. (2019). High-performance subambient radiative cooling enabled by optically selective and thermally insulating polyethylene aerogel. Sci. Adv. *5*, eaat9480.

27. Mandal, J., Fu, Y., Overvig, A.C., Jia, M., Sun, K., Shi, N.N., Zhou, H., Xiao, X., Yu, N., and Yang, Y. (2018). Hierarchically porous polymer coatings for highly efficient passive daytime radiative cooling. Science *362*, 315–319.

28. Gentle, A.R., and Smith, G.B. (2015). A Subambient Open Roof Surface under the Mid-Summer Sun. Adv. Sci. (Weinh.) *2*, 1500119.

29. Yang, P., Chen, C., and Zhang, Z.M. (2018). A dual-layer structure with record-high solar reflectance for daytime radiative cooling. Sol. Energy *169*, 316–324.

30. Zhai, Y., Ma, Y., David, S.N., Zhao, D., Lou, R., Tan, G., Yang, R., and Yin, X. (2017). Scalable-manufactured randomized glass-polymer hybrid metamaterial for daytime radiative cooling. Science *355*, 1062–1066.

31. Kou, J., Jurado, Z., Chen, Z., Fan, S., and Minnich, A.J. (2017). Daytime radiative cooling using near-black infrared emitters. ACS Photonics *4*, 626–630.

32. Li, T., Zhai, Y., He, S., Gan, W., Wei, Z., Heidarinejad, M., Dalgo, D., Mi, R., Zhao, X., Song, J., et al. (2019). A radiative cooling structural material. Science *364*, 760–763.

33. Ruan, X., Li, X., Huang, Z., and Peoples, J.A. (2019). WO2020072818 – Metal-free Solar-reflective Infrared-emissive Paints and Methods of Producing the Same. Patent application no. PCT/US2019/054566, filed October 3, 2019, and published April 9, 2020.

34. Diebold, M.P. (2014). Application of Light Scattering to Coatings: A User's Guide (Springer).

35. Ghosh, G. (1999). Dispersion-equation coefficients for the refractive index and birefringence of calcite and quartz crystals. Opt. Commun. *163*, 95–102.

36. Berdahl, P., and Bretz, S.E. (1997). Preliminary survey of the solar reflectance of cool roofing materials. Energy Build. *25*, 149–158.

37. Frisvad, J.R., Christensen, N.J., Jensen, H.W., Frisvad, J.R., Christensen, N.J., and Jensen, H.W. (2007). Computing the scattering properties of participating media using Lorenz-Mie theory. ACM Transactions on Graphics: Proceedings of the International Conference on Computer Graphics and Interactive Techniques (ACM Press), p. 60.

38. Kaviany, M. (2012). Principles of Heat Transfer in Porous Media (Springer).

39. Liu, C., Wu, Y., Wang, B., Zhao, C.Y., and Bao, H. (2019). Effect of atmospheric water vapor on radiative cooling performance of different surfaces. Sol. Energy *183*, 218–225.

40. ASTM (2013). ASTM E1980-11 Standard Practice for Calculating Solar Reflectance Index of Horizontal and Low Sloped Opaque Surfaces (ASTM).

41. ASTM (2010). D4060, Standard Test Method for Abrasion Resistance of Organic Coatings by the Taber Abraser (ASTM).

42. Hook, J.W., Jacox, P.J., and Spence, J.W. (1994). Acid rain effects on the exterior durability of architectural coatings on wood. Prog. Org. Coat. *24*, 175–188.

43. Whittingstall, P. (2011). Paint Evaluation Using Rheology (TA Instruments).

44. Akbari, H., Levinson, R., and Rainer, L. (2005). Monitoring the energy-use effects of cool roofs on California commercial buildings. Energy Build. *37*, 1007–1016.

45. Mandal, J., Yang, Y., Yu, N., and Raman, A.P. (2020). Paints as a Scalable and Effective Radiative Cooling Technology for Buildings. Joule *4*, 1350–1356.

46. ASTM (2020). Standard Tables for Reference Solar Spectral Irradiances: Direct Normal and Hemispherical on 37° Tilted Surface. Active Standard ASTM G173 (ASTM).